Journal of Magnetic Resonance **150,** 105–109 (2001)
doi:10.1006/jmre.2001.2330, available online at http://www.idealibrary.com on IDEAL®

Electron Spin Relaxation via Vibronic Level of Rhodium(II) Hexacyanide Complex in KCl Crystal

J. A. Coelho Neto and N. V. Vugman

Instituto de Física, Universidade Federal do Rio de Janeiro, Rio de Janeiro 21910-240, RJ, Brazil

Received July 6, 2000; revised March 15, 2001; published online May 10, 2001

Electron spin–lattice relaxation rates for the low-spin $[Rh(CN)_6]^{4-}$ complex in KCl were measured by the inversion recovery and saturation recovery techniques, in the range of 5 to 30 K. Angular variation experiments indicate that electron spin–lattice relaxation times present axial symmetry. The data fit very well to a relaxation process involving localized anharmonic vibration modes, also responsible for the *g* tensor temperature dependence.

I. INTRODUCTION

In the literature there are widely accepted models for electron spin–lattice relaxation processes that involve low frequency transitions. The resonant two-phonon electron spin–lattice relaxation process, postulated independently by Orbach (*1*) and Aminov (*2*), involves absorption of a phonon by a direct process to excite a spin system to a much higher electronic level, at an energy Δ above the ground doublet, followed by the emission of another phonon of slightly different energy so that the magnetic ion is indirectly transferred from one level to the other of the ground doublet (*3*) split by the Zeeman interaction. This process may be considered a predominant electron spin–lattice relaxation pathway when the energy difference Δ is less than the maximum phonon energy available. The electron spin–lattice relaxation rate is shown to depend on temperature (*4*) through the Bose factor,

$$1/T_1 = A[\exp(\Delta/kT) - 1]^{-1}. \qquad [1]$$

At low temperatures, when $\Delta > kT$, this function approaches an exponential dependence $1/T_1 = A\exp(-\Delta/kT)$.

Apart from describing the temperature dependence of this electron spin–lattice relaxation process, fitting the experimental data to this exponential-like function can yield the energy position of an excited paramagnetic level, which might otherwise be unobservable. In the literature there are many examples of the determination of Δ from T_1 measurements employing nonresonant as well as resonant methods, including CW and pulsed electron paramagnetic resonance (*4*, *5*). The measurements are related to paramagnetic rare earth ions or other high spin complexes because the weakness of the crystal field in these systems provides an appropriate low lying ionic excited state.

The experimentally observed exponential-like increase in the electron spin–lattice relaxation rate at low temperatures is not only characteristic for Orbach-type electron spin–lattice relaxation. An alternative is the Murphy-type electron spin–lattice relaxation (*6*), related to a local vibrational mode (internal or external). This can be described as a phonon absorption resulting in simultaneous transition of a local vibration and spin–flip in a double-well tunneling model. This mechanism leads to the temperature dependence,

$$1/T_1 = A\,\mathrm{csch}(\Delta/kT), \qquad [2]$$

with Δ being the tunneling frequency. At low temperatures when $\Delta > kT$ this function approaches an exponential dependence $1/T_1 = A\exp(-\Delta/kT)$.

Neither Orbach–Aminov nor Murphy relaxation processes rely on the Jahn–Teller effect; the Born–Oppenheimer approximation is assumed to be valid.

The Jahn–Teller effect was first postulated to explain the lowering in symmetry of octahedral complexes (*7*) and then to explain the temperature dependence of the *g* and hyperfine tensors that appear in the spin Hamiltonian used to interpreted electron paramagnetic resonance spectra (*3*). This is a direct consequence of the crystal field model for molecules. Nowadays, with the development of sophisticated molecular ab initio calculations which are able to include some of the host lattice as well (*8*), it is possible to show that an axial distortion may arise as a natural consequence of chemical bonding.

For example, an axial distortion represents a minimum in the potential hypersurface of the $[Rh(CN)_6]^{4-}$+ vacancy complex in KCl host lattice; there is a loosening of the coordination bonding between the metal and the axial cyanides, a consequence of the anti-bonding character of the nondegenerate d_{z^2} unpaired electron orbital (*9*). Clearly, there is no need to invoke the Jahn–Teller effect to understand the lowering in symmetry in this case: it is seen as a consequence of chemical bonding. Of course the dynamic Jahn–Teller effect is not to be expected for a nondegenerate ground state.

1090-7807/01 $35.00

Concerning Jahn–Teller systems, electron spin–lattice relaxation via vibronic levels for $Cu(H_2O)_6$ complexes was clearly stated by Williams *et al.* (*10*) and the electron phase relaxation due to excitations to vibronic levels was mentioned by Bill and Silsbee (*11*) and experimentally observed by Hoffmann and coworkers (*12*).

On the other hand, for non Jahn–Teller systems, low frequency vibrational modes were invoked to explain electron spin–lattice relaxation of defects in crystalline quartz (*13*) and of atomic-hydrogen centers generated in fused silica by gamma-irradiation (*14*).

In this paper we report electron spin–lattice relaxation measurements on the $[Rh(CN)_6]^{4-}$ complex in KCl host lattice. We suggest that experimental data can be explained with a relaxation process intermediated by local anharmonic vibrations as deduced before (*15*) from the *g* value's temperature dependence.

II. EXPERIMENTAL

The paramagnetic complex under study is produced by X-ray or 2 Mev electron irradiation on KCl single crystals (*16*) doped with a 0.5% molar proportion of $K_3Rh(CN)_6$. The crystals were grown from slow evaporation of a saturated aqueous solution of KCl to which the desired molar proportion of the salt was added. The EPR experiments were performed at X-band (9.68 GHz) on a Bruker ESP380E pulsed spectrometer using a dielectric cavity inserted into an Oxford CF-935 variable temperature cryostat. The cubic crystals were mounted on a small Teflon cylinder into a quartz tube. The sample was aligned in such a way that one of the principal axes of the cubic crystal is perpendicular to the magnetic field so that one can obtain both the parallel and the perpendicular features of the spectrum with the magnetic field parallel to either of the other axes.

The EPR spectra of this $4d^7$ low spin complex reveal a hyperfine interaction between the unpaired electron occupying a d_{z^2} antibonding orbital and the rhodium nucleus ($I = 1/2$), besides a superhyperfine interaction with two equivalent nitrogens of the axial cyanides. Both *g* and hyperfine tensors are anisotropic and their temperature dependence is attributed to the presence of localized anharmonic vibrations (*15, 17*). Using a selection technique based on T_2 (spin–spin relaxation time) (*18*) we verified the existence of two distinct paramagnetic species, attributed to distinct positions of the charge compensating positive ion vacancy.

Electron spin–lattice relaxation times were measured using an inversion recovery (IR) technique in the temperature range 7–30 K. Temperatures were carefully measured with a calibrated thermocouple located very close to the resonant cavity. The pulse sequence employed was a 56-ns inversion pulse followed by a 400-ns $\pi/2$ pulse. Detection was carried out on the top of the free induction decay signal.

Spectral diffusion is minimized with the application of a sufficiently nonselective inversion pulse and a selective measurement pulse. As a test of the impact of spectral diffusion, the recovery time constant was measured as a function of the inversion pulse width in the range 56–400 ns; the variation was found within the experimental error.

Saturation recovery (SR) experiments were performed at Denver University at 5, 7, and 10 K. At 10 K, using a 5-μs pumping pulse, SR experiments give the same spin–lattice relaxation times as those obtained by the IR method, while at 7 K SR T_1's are about 25% smaller, probably due to two reasons: the larger time window accessible to SR experiments provides better exponential fittings and just a small inaccuracy in the temperature measurement can give rise to significant deviations on the measured T_1 values for the system under study. It is known that below 10 K the temperature in the sample is rather sensitive to the helium flux and to sample thermalization; direct reading may differ from that of a thermocouple located close to the sample. Typical saturation and inversion recovery curves are shown in Fig. 1 at 10 K.

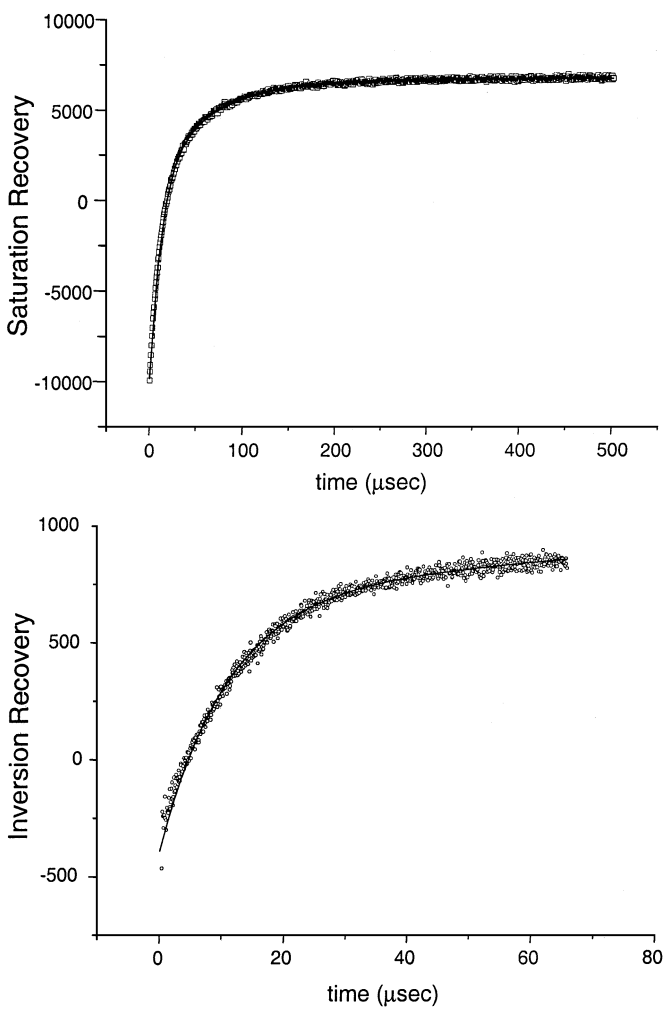

FIG. 1. Typical saturation recovery (top) and inversion recovery (bottom) curves taken at 10 K from the perpendicular EPR spectrum, $\theta = 90°$, of the $[Rh(CN)_6]^{4-}$ complex diluted in a KCl host lattice.

III. RESULTS

The best results are obtained when the experimental data are fitted to two exponentials instead of one, as a consequence of the existence of the two distinct paramagnetic species mentioned above. This is clear from the SR experiments. The first species is more intense and relaxes faster (*18*). The second species is characterized by a rather large electron spin–lattice relaxation time and by a smaller intensity, implying a much lower accuracy in its determination as a consequence of the restricted time window accessible to the IR experiments. Furthermore, the presence of the second exponential in the fitting also implies a lower precision in the determination of the parameters of the first one. For this reason the low intensity slow relaxing exponential was approximated to a linear function in order to get the electron spin–lattice relaxation times from the predominant exponential as a function of temperature. This procedure diminishes the number of parameters and improves the fitting accuracy.

Figure 2 shows the measured temperature dependence of the electron spin–lattice relaxation rate at the parallel ($\theta = 0^\circ$) and the perpendicular ($\theta = 90^\circ$) orientations. A very good fitting to a Boltzmann factor is obtained for both curves with $\Delta = (34 \pm 1)$ cm^{-1}. The SR experimental point at 5 K, measured for $\theta = 90^\circ$, fits well to the IR curve, considering that the temperature at the sample could be 5.5 instead of 5 K, as shown with triangles in Fig. 2.

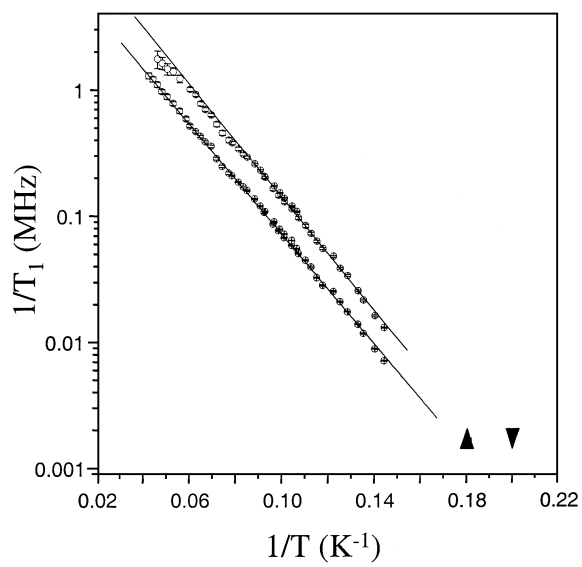

FIG. 2. Temperature dependence of the electron spin–lattice relaxation rate for the $[Rh(CN)_6]^{4-}$ complex diluted in a KCl host lattice for the faster relaxing species, measured by the inversion recovery method. The point at 5 K, represented by a down triangle, was measured by the saturation recovery technique at Denver University; the up triangle represents the same measurement if the temperature is corrected to 5.5 K. The Boltzmann fitting relations are also shown. The upper curve represents data taken at $\theta = 0^\circ$ and the lower curve represents data taken at $\theta = 90^\circ$. The energy separation Δ is found to be (34 ± 1) cm^{-1} for both curves.

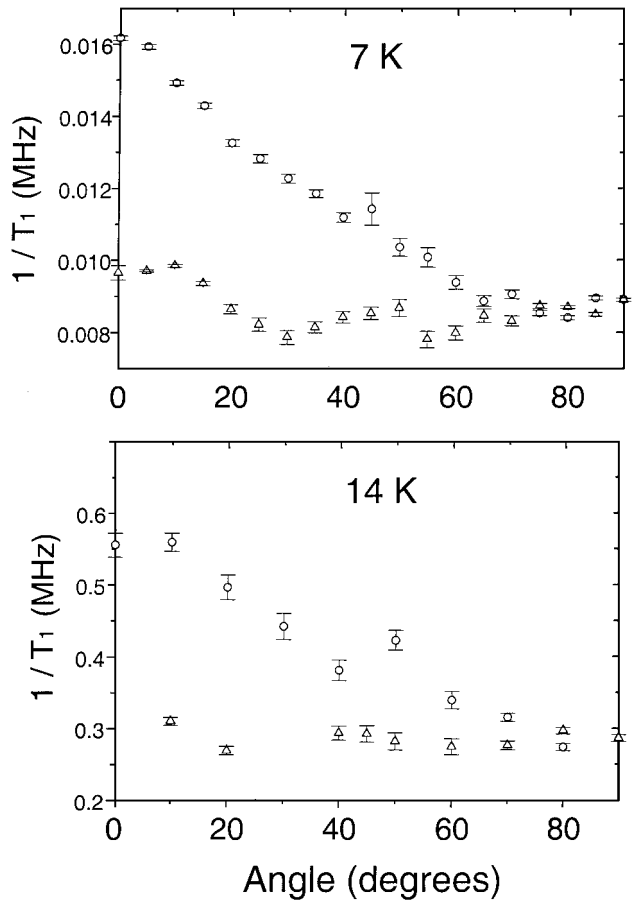

FIG. 3. Angular variation experiments performed at 7 (top) and at 14 K (bottom). The sample was initially aligned in such a way that one of the principal axes of the cubic crystal is perpendicular to the static magnetic field, so that one can obtain both the parallel and the perpendicular features of the spectrum with the magnetic field parallel to either of the other axes. Circles represent data taken in the ZX plane and triangles represent data in the plane YX. Fluctuations in experimental points are mainly due to temperature fluctuations.

Angular variation experiments, performed at two distinct temperatures, are shown in Fig. 3. The observed anisotropy is far too large to be attributed solely to the Zeeman interaction, which is mainly responsible for the electron spin–lattice relaxation mechanism; the electron spin–lattice relaxation process, therefore, must also depend on the angle between the external magnetic field and the complex principal symmetry axis. Measurement of T_1 as a function of the magnetic field under the parallel spectrum demonstrates a complete independence on M_i, ruling out hyperfine interactions as possible electron spin–lattice relaxation mechanisms.

There is a prediction that Orbach electron spin–lattice relaxation rates of Kramers' ions should show some angular anisotropy (*19*), somewhere around 50% (calculated for trivalent neodymium). In fact, a much larger anisotropy (a factor of 12) was reported (*20*) for trivalent Nd in $La_2Mg_3(NO_3)_{12} \cdot 24\,H_2O$. The observed angular dependence, in our case, reveals an

anisotropy of about 50% and a functional shape similar to that predicted (*19*) for the direct process in a sample of 1% Ce^{3+} in $LaCl_3$. Modeling this effect is beyond the scope of this work.

IV. VIBRONIC ELECTRON SPIN–LATTICE RELAXATION PROCESS

In the usual treatment of the temperature dependence of electron spin–lattice relaxation of impurity ions, the vibrational properties of the paramagnetic ion are assumed to be those of a normal host ion. For impurities that do not affect the vibrational properties of the lattice, this is expected to be a reasonable approximation. However, if a paramagnetic impurity is associated with a gross defect in a crystal, it should be expected that the temperature dependence of the electron spin–lattice relaxation time would be dominated by the vibrational properties of the defect. An ion could be trapped at a site about which the potential is highly anharmonic such that the vibrational amplitude is very large. Under these circumstances, lattice vibrations could beat the localized vibrations, producing a difference frequency resulting in a spin transition in a process similar to Murphy's relaxation (*6*) but in a single well.

As mentioned above, low frequency localized anharmonic modes were inferred from the *g* tensor temperature dependence for the paramagnetic species under study. Two vibration modes (*15*) are reported, with A_{2u} and A_{1g} symmetry, respectively, with frequencies of 37 and 50 cm^{-1} (10% estimated error).

Vibronic coupling between the A_{1g} electronic ground state to these modes must be considered and will give rise to the energy levels relevant to the relaxation problem. Figure 4 illustrates this idea, considering only one vibration mode. The resonant excited state is now a vibronic level and not an excited electronic one as in the Orbach–Aminov process. Dotted lines indicate the coupling to lattice phonons and ΔE is the usual Zeeman energy. The expected temperature dependence, as the population of the vibronic levels is determined by the Boltzmann statistics, is not through the Bose factor but follows an exponential law as

$$1/T_1 = A\exp(-\Delta/kT). \qquad [3]$$

The Δ value obtained in this work suggests that the reported (*15*) lower frequency mode is mainly responsible for the measured electron spin–lattice relaxation process. This is an odd parity mode, if we consider a D_{4h} local symmetry. According to theory based on harmonic vibration modes (*21*), when there is an inversion center, electron spin–lattice relaxation is sensitive to local modes which are even under inversion. In this case the known anharmonicity of the local vibration modes will

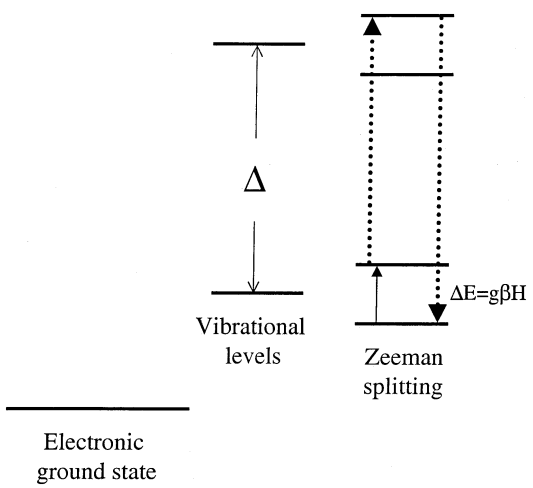

FIG. 4. Energy levels relevant to the vibronic electron spin–lattice relaxation. Instead of an electronic excited state such as the Orbach–Aminov process, the electron spin–lattice relaxation process is governed by the coupling between the electronic system and localized anharmonic vibrations. Dashed lines indicate the coupling to lattice phonons and ΔE is the usual Zeeman energy. The diagram is not to scale and the interactions have been depicted successively in the following order: pure electronic, vibronic (taking into account the zero point energy), and vibronic plus Zeeman.

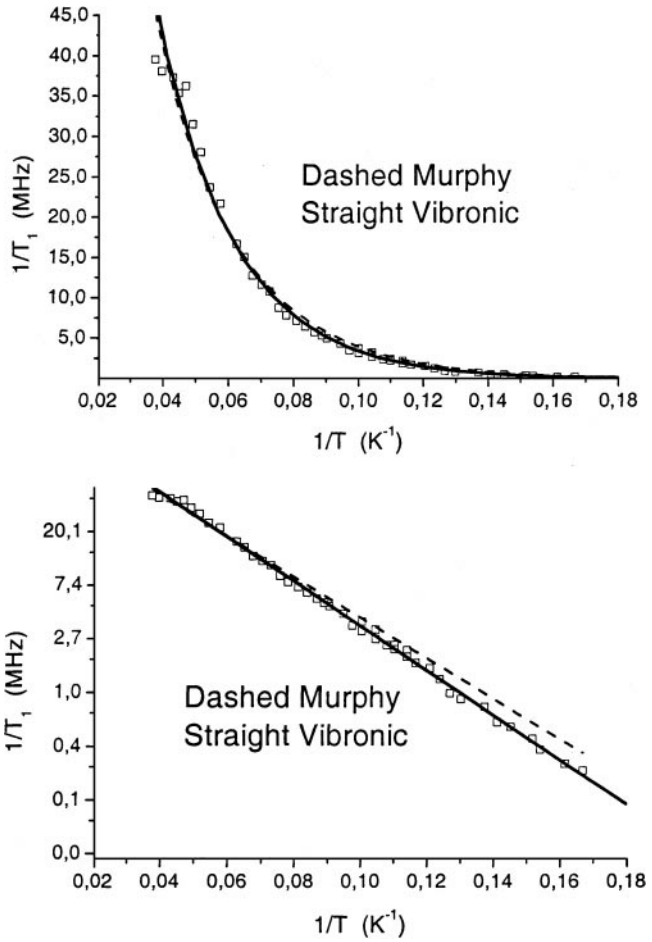

FIG. 5. Comparison between the vibronic model electron spin–lattice relaxation process and Murphy's model. The logarithmic plot (bottom) of the relaxation rate as a function of the reciprocal temperature unravels the differences which are hidden in a linear plot (top).

introduce odd components in the vibronic Hamiltonian, making the parity of its eigenfunctions undetermined and providing nonnull matrix elements of the orbit–lattice operator. Furthermore, symmetry lowering caused by the presence of the charge compensating vacancy also plays a role in electron spin–lattice relaxation.

The higher frequency mode might also contribute to electron spin–lattice relaxation in the temperature range in which the experiment was performed. A combined decay remains exponential while the rate constants for the two electron spin–lattice relaxations add. So we are measuring a resultant relaxation rate, dominated by the lower frequency mode contribution. The excellent agreement between the Δ value estimated from the g value's temperature dependence and the present electron spin–lattice relaxation rates may be rather fortuitous, considering all of the symplifying assumptions involved in the localized anharmonic vibrations model (*17*) and the experimental uncertainties. Nevertheless, there is a clear indication that vibronic relaxation plays a very important role in the measured electron spin–lattice relaxation rates for the paramagnetic $[Rh(CN)_6]^{4-}$ complex in KCl host lattice.

Finally, we reference to Murphy's relaxation process. Electron spin–lattice relaxation via this process and via vibronic levels is not easily distinguishable at low temperatures. Figure 5 depicts the best fitting to the experimental data according to the two models: the logarithmic plot indicates that Murphy's process gives a poorer fitting in our case. On the other hand, it is hard to imagine a physically meaningful double well for a cubic host lattice without invoking a strong Jahn–Teller deformation, which is not possible for a nondegenerated ground state.

ACKNOWLEDGMENTS

This work was cosponsored by FINEP and FUJB-UFRJ. The authors are indebted to CNPq for a research fellowship (NVV) and for a Ph.D. fellowship (JACN). We thank Prof. G. Eaton and Prof. Sandra Eaton for the saturation recovery measurements and Dr. A. A. Leitão for useful discussions. We thank Dr. R. B. Capaz for useful suggestions in the manuscript.

REFERENCES

1. R. Orbach, *Proc. R. Soc. A* **264,** 485 (1961).
2. L. K. Aminov, *Zh. Eksp. Teor. Fiz*. **42,** 783 (1962).
3. A. Abragam and B. Bleaney, "Electron Paramagnetic Resonance of Transition Metal Ions," Clarendon Press, Oxford, 1970.
4. R. Orbach and H. J. Stapleton, *in* "Electron Paramagnetic Resonance" (S. Geshwind, Ed.), p. 121, Plenum Press, New York, 1971.
5. M. W. Makinen, L. C. Kuo, M. B. Yim, G. B. Wells, J. M. Fukuyama, and J. E. Kim, *J. Am. Chem. Soc*. **107,** 5245 (1985).
6. J. Murphy, *Phys. Rev*. **145,** 241 (1966).
7. H. A. Jahn and E. Teller, *Proc. Royal Soc. A* **161,** 220 (1937).
8. A. A. Leitão, J. A. Coelho Neto, N. M. Pinhal, C. E. Bielschowsky, and N. V. Vugman, *J. Phys. Chem*. **105,** 614 (2001).
9. A. A. Leitão, N. V. Vugman, and C. E. Bielschowsky, *Chem. Phys. Lett.* **321,** 269 (2000).
10. F. I. B. Williams, D. C. Krupka, and D. P. Breen, *Phys. Rev.* **179,** 255 (1969).
11. H. Bill and R. H. Silsbee, *Phys. Rev. B* **10,** 2697 (1974).
12. S. K. Hoffmann, J. Goslar, W. Hilczer, M. A. Augustyniak, and M. Marciniak, *J. Phys. Chem. A* **102,** 1697 (1998).
13. J. G. Castle Jr. and D. W. Feldman, *Phys. Rev. A* **137,** 671 (1965).
14. D. W. Feldman, J. G. Castle Jr., and G. R. Wagner, *Phys. Rev.* **145,** 237 (1966).
15. N. V. Vugman and W. O. Franco, *Phys. Lett. A* **155,** 516 (1991).
16. N. V. Vugman and W. O. Franco, *J. Chem. Phys.* **78,** 2099 (1983).
17. N. V. Vugman and M. Rothier Amaral, Jr., *Phys. Rev.* **42,** 9837 (1990).
18. J. A. Coelho Neto and N. V. Vugman, *J. Magn. Reson.* **125,** 242 (1997).
19. R. C. Mikkelson and H. J. Stapleton, *Phys. Rev.* **140,** 1968 (1965).
20. G. H. Larson and C. D. Jeffries, *Phys. Rev.* **145,** 311 (1966).
21. J. H. Van Vleck, *Phys. Rev.* **57,** 426 (1940).